Biomechanics and Modeling in Mechanobiology (2020) 19:251–261
https://doi.org/10.1007/s10237-019-01208-3

ORIGINAL PAPER

Deformation of human red blood cells in extensional flow through a hyperbolic contraction

Mohammad M. Faghih[1] · **M. Keith Sharp**[1]

Received: 2 April 2019 / Accepted: 24 July 2019 / Published online: 6 August 2019

Abstract
Flow-induced damage to red blood cells has been an issue of considerable importance since the introduction of the first cardiovascular devices. Early blood damage prediction models were based on measurements of damage by shear stress only. Subsequently, these models were extrapolated to include other components of the fluid stress tensor. However, the expanded models were not validated by measurements of damage in response to the added types of stress. Recent investigations have proposed that extensional stress might be more damaging to red cells than shear stress. In this study, experiments were conducted to compare human red cell deformation under laminar extensional stress versus laminar shear stress. It was found that the deformation caused by shear stress is matched by that produced by an extensional stress that is approximately 34 times smaller. Assuming that blood damage scales directly with cell deformation, this result indicates that mechanistic blood damage prediction models should weigh extensional stress more than shear stress.

Keywords Red blood cell · Extensional stress · Deformation index · Hyperbolic contraction · Hemolysis · Power-law model · Mechanical blood damage · Scalar stress

1 Introduction

Since the introduction of the first implantable blood-contacting devices, flow-induced hemolysis has been the focus of many research studies (Faghih and Sharp 2019a). Historically, it was assumed that shear stress and exposure time are the two main factors responsible for the hemolysis (Blackshear et al. 1965; Heuser and Opitz 1980; Leverett et al. 1972). Therefore, the effect of shear stress has received considerable attention in the literature (Brown et al. 1975; Giersiepen et al. 1989; Laugel and Beissinger 1983; Leverett et al. 1972; Nevaril et al. 1968; Richardson 1974).

As one of the first attempts to correlate shear stress and exposure time to the level of hemolysis, hemoglobin release was measured after applying a range of shear stresses to blood samples in a viscometer (Heuser and Opitz 1980). The result was the popular power-law model. Several other authors have performed similar experiments on blood samples of various species (Ding et al. 2015; Zhang et al. 2011). Because of its simplicity, there has been an inclination toward using the power-law model for flow conditions other than pure shear. To use the power-law model in more complex geometries, where multiple components of the fluid stress tensor may be nonzero, a scalar stress was introduced (Bludszuweit 1995; Faghih and Sharp 2016). The scalar stress is a von Mises-like stress that weighs the components of the fluid stress tensor with the same proportions as mechanical stresses in common solid materials. That the response of a red cell to fluid stresses is identical to that of, say, a steel beam to mechanical stresses is questionable (Faghih and Sharp 2019a).

The appropriateness of applying the scalar stress for hemolysis prediction in flows other than pure shear has been modeled (Faghih and Sharp 2018a). Cell membrane tension for the same scalar stress value was compared in five cases, namely laminar shear, laminar extension, turbulent shear with the cell tank-treading inside an eddy, turbulent shear with the cell between two corotating eddies, and turbulent extension with the cell between two counter-rotating eddies. The results, which were reported for both eddies of the highest energy content and for Kolmogorov eddies, showed that the membrane tensions varied by more than two orders of magnitude among the different cases. This mismatch implies

✉ M. Keith Sharp
keith.sharp@louisville.edu

[1] Biofluid Mechanics Laboratory, Department of Mechanical Engineering, University of Louisville, Louisville, USA

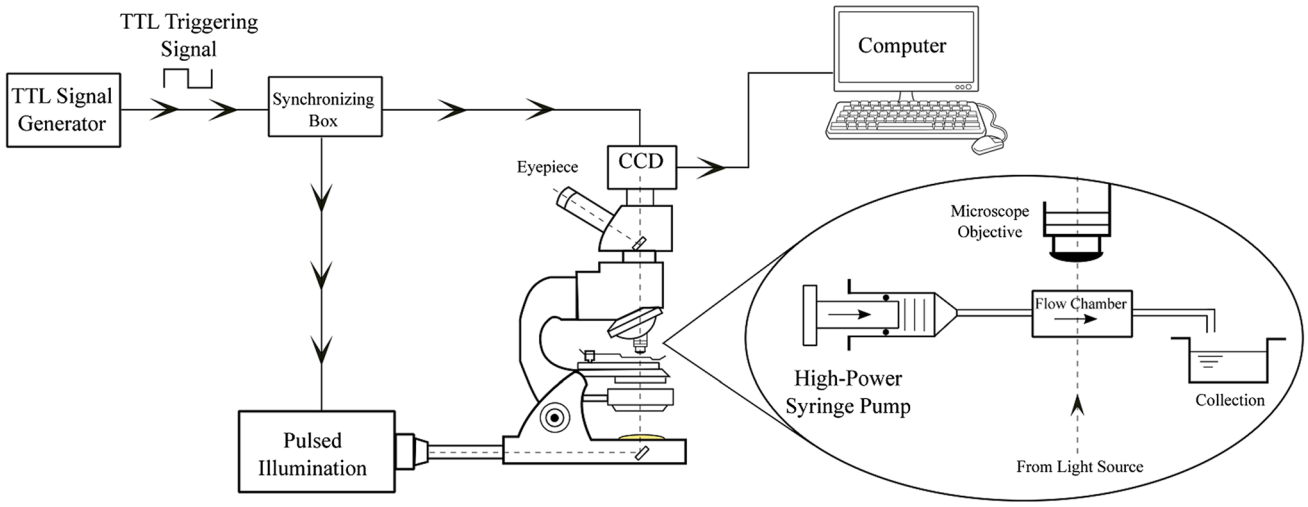

Fig. 1 Schematic of the experimental setup to capture images of RBCs flowing through channels

that scalar stress, with the current weighting factors for different components of the stress tensor, may not be a good predictor of hemolysis. Similarly, unfavorable results were also obtained when the five cases mentioned above all have the same energy dissipation rate equivalent stress (Faghih and Sharp 2019b). Therefore, to provide a better representative stress to scale hemolysis, the behavior of red blood cells (RBCs) in flow conditions beyond pure shear needs to be quantified. Interested readers are advised to read the recent review article by Faghih and Sharp (2019a) for a discussion on blood damage modeling.

Recently, increasing attention has been placed on the effect of extensional stress on RBC damage. Computational fluid dynamics simulations have been used to examine capillary flow with different types of entrances, and a range of viscosities and flow rates (Down et al. 2011). Results showed that the shear stress in the flow domain failed to reach the threshold level consistent with the experimental values of hemolysis reported by Keshaviah (1976). However, the extensional stress at the entrance region reached or exceeded a stress threshold of 3000 Pa and lasted for a duration on the order of microseconds. Experimental results comparing the flow in tubes with sharp and tapered entrances have indicated that hemolysis is better correlated with extensional stress than shear stress (Yen et al. 2015). Even in a rotary blood pumps, in which shear stress might be expected to dominate, normal stresses are significant (Khoo et al. 2018).

Analyzing the motion and deformation of RBCs under different flows (i.e., shear, extension, and combinations of the two) can promote understanding of how the cell membrane might be damaged in response to fluid stresses. In a pure shear flow, where the viscosity and shear rate are large enough, the RBCs tend to assume an elongated shape with their longer axis angled in the direction of the flow, while the membrane rotates around the cell contents (i.e., tank-treading motion) (Basu et al. 2011; Dupire et al. 2012).

Deformation of RBCs in pure shear flow has also been investigated by several authors (Chen and Sharp 2011; Fischer et al. 1978; Pfafferott et al. 1985). However, deformation of RBCs in extensional flow has received little attention. One of few studies on RBC motion under extensional stress was performed by Lee et al. (2009), who carried out experiments on rabbit RBCs to investigate the difference in cell response to shear and extensional stress. It was found that the cells deform more easily in extensional stress than in shear stress at the same stress level. However, the comparison was made up to a stress level of only around 3 Pa. The present study aims to measure the deformation of human red blood cells in shear versus extensional stress of an order of magnitude larger than those by Lee et al. (2009).

2 Materials and methods

2.1 Experimental setup

Images were captured of RBCs in shear and extensional flow in small-scaled channels (Fig. 1). The flow channels were composed of three poly(methyl methacrylate) (PMMA) sheets (McMaster-Carr Co., Elmhurst, USA) with thickness of 1/32 inch (0.794 mm). The channel geometries were machined into the middle sheet. The top sheet incorporated inlet and outlet ports with threaded PMMA blocks. A featureless bottom sheet closed each channel.

A hyperbolic contraction is unique in that it imposes a constant extensional strain rate along its centerline (Oliveira et al. 2007; Sousa et al. 2011a, b). The hyperbolic contraction

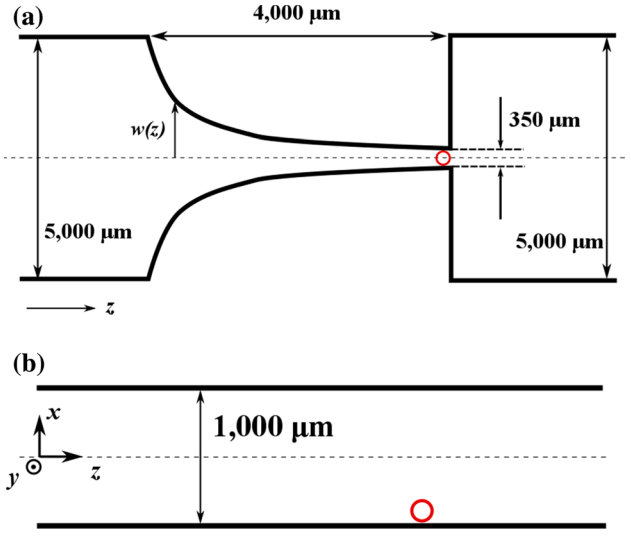

Fig. 2 Schematic of **a** the hyperbolic flow channel used in this study to exert extensional stress to RBCs and **b** the rectangular channel for pure shear flow; red circles show the fields of view where images were taken

used in this study started with a width of $w_u = 5$ mm and continued for length $L_c = 4$ mm to reach a width of $w_d = 0.35$ mm at the end of the contraction and finally was followed by an abrupt expansion to the same width as the beginning of the contraction (Fig. 2a). The depth of the channel was $d = 0.794$ mm.

The extension rate ($\dot{\varepsilon}$) for a continuum fluid along the centerline of the hyperbolic channel can be calculated as (Lee et al. 2009; Ober et al. 2013; Oliveira et al. 2007)

$$\dot{\varepsilon} = \frac{Q}{L_c d}\left(\frac{1}{w_d} - \frac{1}{w_u}\right) \tag{1}$$

where Q is the flow rate through the channel. The length of the upstream section of the hyperbolic channel was designed to be long enough for the flow to become fully developed before entering the contraction. The field of view for capturing images was at the end of the contracting region, at mid-depth inside the channel, to ensure that only extensional flow acted on the cells.

For the shear flow, a simple flow channel with a rectangular cross section was fabricated (Fig. 2b). The width of the channel was $w_s = 1$ mm, and the depth was $d = 0.794$ mm.

The field of view for the pure shear case was the region near the bottom wall ($x = 0.5$ mm), at mid-depth ($y = 0$) inside the channel (red circle in Fig. 2b). Again, the length of the shear channel, from the beginning to the image-recording point, was chosen to be more than that required for fully developed flow.

The velocity profile for the rectangular channel is (White 1991)

$$v_z(x,y) = \frac{48Q}{w_s d}\frac{\sum_{i=1,3,5,\ldots}^{\infty}(-1)^{\frac{i-1}{2}}\cos(i\pi x/w_s)\left(1-\frac{\cosh\left(\frac{i\pi y}{w_s}\right)}{\cosh\left(\frac{i\pi d}{2w_s}\right)}\right)}{\left(1-\frac{192w_s}{\pi^5 d}\sum_{i=1,3,5,\ldots}^{\infty}\frac{\tanh(i\pi d/2w_s)}{i^5}\right)} \tag{2}$$

where v_z is the streamwise velocity, Q is the flow rate in the channel, w_s is the width of the channel, and d is the depth of the channel. Since the RBCs were imaged at mid-depth inside the channel, $y = 0$ in Eq. (2). According to the location of the RBC with respect to the wall (i.e., different x), Eq. (2) and its derivative were used to calculate the velocity and shear rate at the corresponding point.

Solvent-based bonding was used to assemble the channels, which is explained in detail elsewhere (Faghih and Sharp 2018b). In short, the surfaces were first washed with deionized water and treated by corona surface treatment to improve the bonding. Then, a solvent (80% isopropanol and 20% dichloromethane) was applied to the mating surfaces and the parts were pressed together under a force of 50 kN. Finally, the parts were annealed in an oven with a uniform temperature of 70 °C for about 5 min. One of the issues that prevented Lee et al. (2009) from testing at higher stresses was that their channel leaked at high flow rates. The solvent-based bonding method used in this project enabled high flow rates without any leakage.

A syringe pump was built in-house to provide the necessary flow rate to reach stress levels exceeding those of previous experiments. The syringe pump utilized an electric motor (Bodine Electric Company, Northfield, IL) with a variable RPM setting to provide a range of flow rates. The fabricated syringe holder was capable of accommodating three 140-ml syringes. The minimum and maximum flow rates tested during the all experiments were 0.888 ml/s and 6.55 ml/s, respectively.

A Zeiss Imager D1 (Thornwood, NY, USA) upright microscope with Köhler illumination was used for imaging the cells moving through the channels. A Nikon extra-long working distance microscope objective, CFI S Plan Fluor ELWD 40X, equipped with a mechanical correction collar was used to focus through the relatively thick top cover to mid-depth in the channel. A monochrome digital camera, QICAM Fast 1394 (QImaging Company, Canada) with best quantum efficiency at wavelengths of 400–600 nm and a frame rate of 5 Hz, was used to record the images.

The Abbe diffraction distance, which gives the smallest resolvable feature within an image, can be calculated by $L_{\text{Abbe}} = 0.53 \times \lambda/\text{NA}$, where λ is the light source wavelength and NA is the numerical aperture of the microscope objective. In the present case, the peak wavelength was around 400 nm and the numerical aperture of the 40× objective was $NA = 0.75$, resulting in $L_{\text{Abbe}} = 0.44\,\mu\text{m}$. This is almost 5.7

times smaller than the smallest dimension of the stretched cell during all the experiments (≈2.510 µm). In addition, pixel oversampling can be calculated as $L_{\text{Abbe}} \times \frac{\text{Magnification}}{\text{Camera pixel size}} = 0.44\,\mu\text{m} \times \frac{40}{4.65\,\mu\text{m}} = 3.8$. Thus, the Abbe diffraction limit was 3.8 over-sampled, which means that pixelation did not limit the resolution of cell dimensions.

To freeze the fast motion of the cells moving though the flow channel, a pulsed light source, Nanolite Driver 2000 (High-Speed Photo-Systeme, Germany), was triggered by an external TTL signal. A Nanolite Nanosecond flash lamp, model KL-M (High-Speed Photo-Systeme, Germany), was connected to the pulsed light generator unit using a BNC cable. The duration of the spark was 11 ns, while the discharged energy was 14 mJ, with a maximum flash rate of 20 kHz. Maximum intensity of the spark from the flash lamp occurred at wavelengths of 400–500 nm. Synchronization between the camera and the light source was accomplished using a LabVIEW (National Instruments, Austin TX) code.

For the 40X microscope objective, one camera pixel dimension (4.65 µm) of motion blur corresponds to a cell velocity of 4.65 µm/11 ns/40 = 10.6 m/s. For smaller velocities, subpixel blur occurs. For the velocity associated with each cell image, the motion blur was calculated and subtracted from the measured dimension of the cell. Motion blur correction was only applied to the streamwise, and not the transverse, direction.

Two human blood samples (adenine–saline (AS-1) added, leukocyte reduced) were provided from the American National Red Cross and the University of Louisville Hospital Blood Bank. The blood samples (anticoagulated with sodium citrate) were already 28 days old when received, but were otherwise healthy. All experiments were performed within 2 days. For the imaging experiments, 1 ml of whole blood was diluted in 100 ml of 0.9% saline water immediately before the experiments. In addition, to reach higher stress levels, the viscosity of the suspending fluid was increased with Dextran-500 (Fisher Scientific Inc., Hampton, NH) (Chen and Sharp 2011; Fischer 2007; Tran-Son-Tay et al. 1987) to 4.2 cP and 11 cP. Higher viscosities also ensured laminar flow. Dextran has been previously shown to cause no damage to RBCs (Fischer 2007; Fischer et al. 1978). The viscosity of the fluid was measured by a cone and plate viscometer (model LVTCP42, Brookfield, Stoughton, MA, USA).

2.2 Uncertainty and statistical analysis

The accuracy of the viscometer measurement was ±0.1 cP. For each viscosity, a total of 10 measurements were done. For the tests on the first blood sample, the total uncertainty (including Type A and Type B uncertainties) for the three viscosities was ±0.12 cP, ±0.11 cP, and ±0.11 cP. Hence, the three values for the viscosities in average ± uncertainty format were 1.03 ± 0.12 cP, 4.16 ± 0.11 cP, and 11.01 ± 0.11 cP. Viscosities for the second blood sample were 1.04 ± 0.14 cP, 4.2 ± 0.12 cP, and 11.04 ± 0.11 cP. Note that these three viscosities are rounded to 1 cP, 4.2 cP and 11 cP in the plots in the following sections.

Channel fabrication and channel measurement uncertainty was ±25 µm. Cell dimensions and distance from the wall had a measurement uncertainty of ±0.1 µm. Precision of 3 significant digits was used throughout the calculations.

All the statistical analyses were performed using Minitab v18 (Minitab INC., State College, PA, USA) with two-sided 95% confidence intervals. For the extensional flow case, one-way analysis of variance (ANOVA) was used to test sample-to-sample differences in aspect ratio at the same stress level. In the shear flow cases, analysis of covariance (ANCOVA) was used to test the difference between aspect ratios among two different viscosities within each blood sample. The same test was used to examine the difference in aspect ratio for the three different viscosities within each blood sample.

2.3 Experimental procedure

All the experiments were performed at room temperature (21 °C).

For extensional flow experiments, only the RBCs that were located within a central band with width of 20 µm in the middle of the channel were selected for measurement. For simplicity, the strain rate for cells within this band was characterized as that along the channel centerline, which is accurate to within ≈4%.

Three different suspending medium viscosities were used for the hyperbolic contraction, namely 1 cP, 4.2 cP, and 11 cP (note that 1 cP = 1 mPa s). Only two viscosities (4.2 cP and 11 cP) were used for shear flow, because the

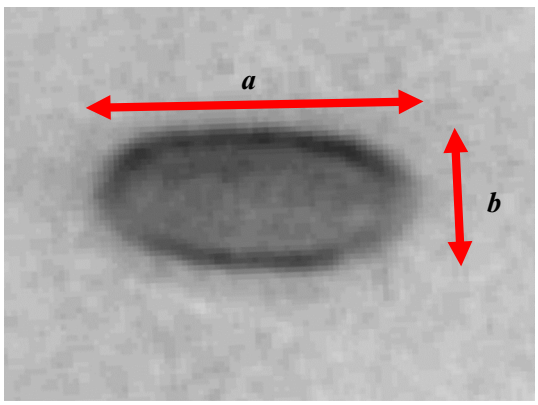

Fig. 3 Measurement of aspect ratio for a red blood cell in extensional flow

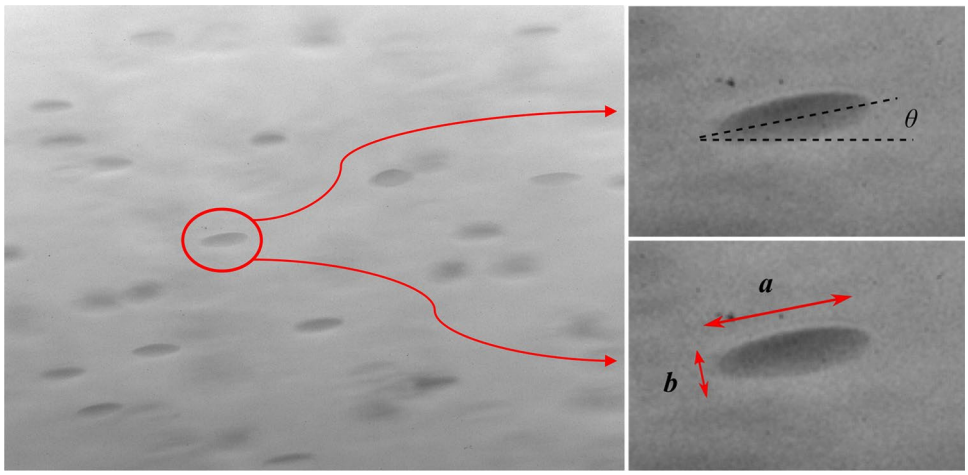

Fig. 4 Measurement of RBC dimension and its tank-treading angle in shear flow

cells in 1 cP fluid tumbled rather than tank-treaded even at the highest shear rate achievable by the pump.

For each experimental case, more than 50 images were captured. More than 30 cells with best image quality of cell boundaries were selected for the final measurement of each experimental run. ImageJ software was used to measure cell aspect ratio, i.e., the ratio of the cell major diameter (a) to cell minor diameter (b) (example of aspect ratio measurement for extensional flow in Fig. 3 and for shear flow in Fig. 4).

For both extensional and shear flows, laminar flow was ensured by limiting the Reynolds number to no more than 2000. After each run of the experiment, the samples were discarded to ensure that the cells were exposed to stress only once.

2.4 Representative stress

Previously, several types of representative stress have been introduced for use in hemolysis prediction models. Among them is the von Mises-like scalar stress (σ_s), written as (Faghih and Sharp 2019a)

$$\sigma_s = \sqrt{\frac{1}{3}\left(\sigma_{xx}^2 + \sigma_{yy}^2 + \sigma_{zz}^2\right) - \frac{1}{3}\left(\sigma_{xx}\sigma_{yy} + \sigma_{xx}\sigma_{zz} + \sigma_{yy}\sigma_{zz}\right) + \left(\tau_{xy}^2 + \tau_{xz}^2 + \tau_{yz}^2\right)} \tag{3}$$

where σ_{ii} is extensional stress and τ_{ij} is shear stress. Another common representative stress is the energy dissipation rate equivalent stress (σ_e) (Faghih and Sharp 2019a)

$$\sigma_e = \sqrt{\frac{1}{2}\left(\sigma_{xx}^2 + \sigma_{yy}^2 + \sigma_{zz}^2\right) + \left(\tau_{xy}^2 + \tau_{xz}^2 + \tau_{yz}^2\right)} \tag{4}$$

However, both of these hypothesized representative stresses lack validation across the range of flows that cells may encounter, with extensional flow being arguably the most important of the neglected cases.

In this study, a first attempt is made to develop a simplified representative stress that accommodates the contrasting responses of cells to shear stress versus extensional stress. Recognizing that the membranes of stretched cells in extensional flow and those of tank-treading cells in shear flow experience distinctly different tensions, the new representative stress applies an empirical weighting factor that scales the ratio of cell deformations by these two different flows

$$\sigma_n = \sqrt{C_n^2\left[\sigma_{xx}^2 + \sigma_{yy}^2 + \sigma_{zz}^2 - \left(\sigma_{xx}\sigma_{yy} + \sigma_{xx}\sigma_{zz} + \sigma_{yy}\sigma_{zz}\right)\right] + \left(\tau_{xy}^2 + \tau_{xz}^2 + \tau_{yz}^2\right)} \tag{5}$$

where C_n is an empirical constant, which is obtained based on the experimental results in this study. The new representative stress has the same form as the von Mises stress [Eq. (3)], except that whereas the von Mises stress predicts that solid materials yield in pure shear for a shear stress that is $\sqrt{3}$ smaller than the extensional stress for planar extension, the new stress predicts that red cells fail in planar extensional flow for an extensional stress that is C_n times smaller than the shear stress for failure in pure shear flow.

In the experiments in this study, only two simple cases, pure shear in the xz plane in the shear channel (τ_{xz}) and planar extensional stress in z direction in the hyperbolic channel $(\sigma_{zz}, \sigma_{xx} = -\sigma_{zz})$, were tested. For these cases, the new representative stress is simplified as

$$\sigma_n = \sqrt{3C_n^2\sigma_{zz}^2 + \tau_{xz}^2} \tag{6}$$

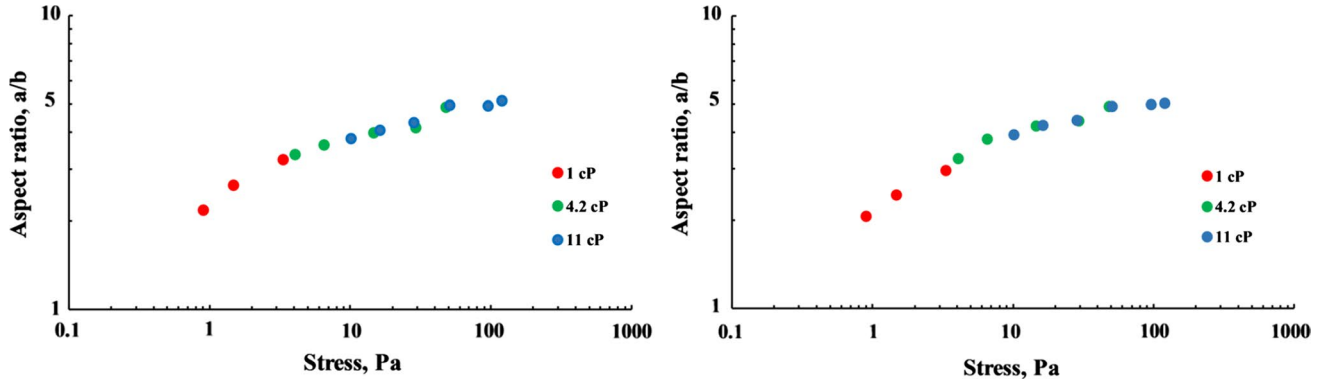

Fig. 5 Measured aspect ratios in extensional flow for three different viscosities for sample 1 (left) and sample 2 (right). *Note*: Both axes have log scales

The objective was to find a value of C_n such that the representative stress accurately scales the cell aspect ratio for both pure shear and planar extension. To do this, first the aspect ratios for shear flow were curve-fitted by a log equation as

$$A_s = c_1 \ln\left(\tau_{xz}\right) + c_2 \tag{7}$$

where A_s is the aspect ratio of the cells in shear flow and c_1 and c_2 are empirical constants. Then, a new set of extensional stresses adjusted by the factor $C_n\left(\sigma_{zz,a}\right)$ were found by plugging the aspect ratio values A_e measured for extensional flow into the curve-fitted equation for shear flow [Eq. (7)].

$$\sigma_{zz,a} = e^{\frac{(A_e - c_2)}{c_1}} \tag{8}$$

Next, the root sum squared (RSS) of the difference between the log of the adjusted extensional stress and the log of the original extensional stress was minimized to calculate the constant value $\left(C_n\right)$ needed to map the original extensional stress to the shear stress data points.

$$\sqrt{\sum_{i=1}^{n}\left(\log\left(\sigma_{zz,a}\right)_i - \sqrt{3}C_n \log\left(\sigma_{zz}\right)_i\right)^2} = \mathrm{RSS} \tag{9}$$

where i is the counter for experimental data points for the extensional stress.

3 Results

3.1 Extensional stress

The aspect ratio of the cells in laminar extensional stress increased as the fluid stress increased, with an asymptotic behavior at higher stresses (Fig. 5). Standard deviation values for the aspect ratio measurements are not included in the plots to increase readability. However, the same information along with the standard deviations is listed in Table 1.

Statistical analysis indicated that the difference between the aspect ratios in the two blood samples at the same stress value was not significant ($p > 0.05$). Furthermore, within each blood sample, higher viscosity did not cause a significant difference in aspect ratio ($p > 0.05$).

3.2 Shear flow

Aspect ratios for blood samples 1 and 2 in shear flow also exhibited similar trends (Fig. 6). Since good cell images occurred over a range of shear stresses associated with different distances from the wall, common shear stresses at which a standard deviation could be calculated were not obtained for shear flow.

Table 1 Aspect ratio of the RBCs for the two blood samples in extensional flow

Viscosity (cP)	Stress (Pa)	Aspect ratio		SD (±)	
		Sample 1	Sample 2	Sample 1	Sample 2
1	0.90	2.17	2.06	0.091	0.118
	1.47	2.63	2.44	0.131	0.087
	3.32	3.22	2.97	0.074	0.090
4.2	4.05	3.36	3.25	0.087	0.073
	6.50	3.61	3.79	0.107	0.080
	14.60	3.98	4.21	0.085	0.076
	29.20	4.14	4.38	0.126	0.038
	47.85	4.88	4.91	0.150	0.064
11	10.14	3.81	3.93	0.092	0.086
	16.22	4.07	4.23	0.137	0.029
	28.33	4.32	4.41	0.066	0.073
	50.67	4.95	4.91	0.109	0.048
	95.33	4.90	4.98	0.124	0.057
	119.67	5.11	5.04	0.082	0.103

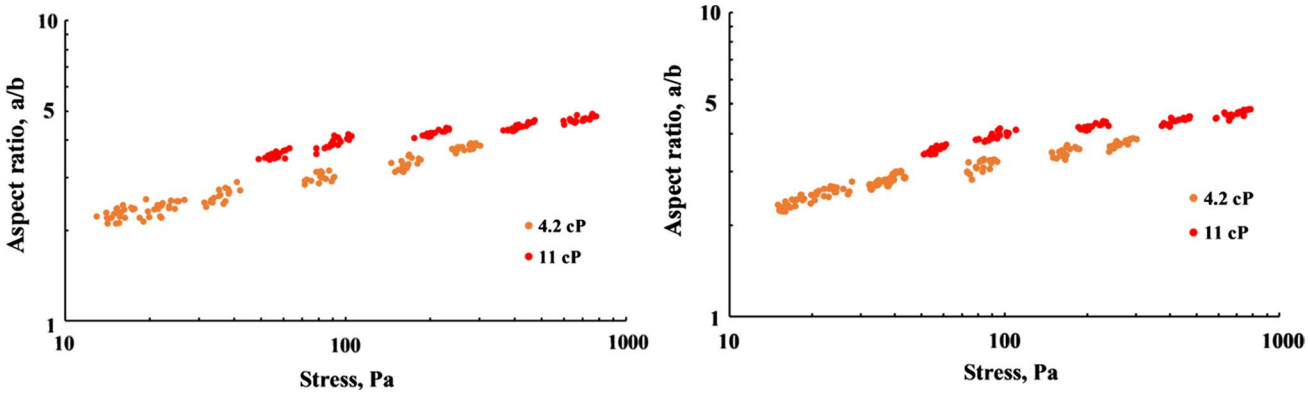

Fig. 6 Aspect ratio of RBCs in shear flow at two different viscosities for sample 1 (left) and sample 2 (right). *Note*: Both axes have log scales

Within each blood sample, a significant difference was observed in aspect ratios between the two different viscosities ($p < 0.05$). This trend has also been observed in previous studies (Mohandas et al. 1980; Pfafferott et al. 1985) (Sect. 4).

3.3 Representative stress

Statistical analysis within each blood sample indicated that there was a significant difference in the aspect ratios between shear stress and extensional stress ($p < 0.05$). Therefore, a universal hemolysis prediction model should incorporate this difference. Assuming that hemolysis scales with the cell aspect ratio, the new scalar stress introduced in Eq. (3) is designed to weight the extensional stresses such that the same level of stress (shear or adjusted extension) gives the same cell deformation.

In other words, the goal is to rescale the horizontal axis in Figs. 5 and 6 such that the data points for extensional stress lie on the same curve as the shear stress data points. To calculate the adjustment factor C_n, the data points for extensional stress for all viscosities were used. However, since the cell aspect ratio for shear flow depends on the suspending medium viscosity, only the data points for the suspending viscosity of 4.2 cP were used, because it is closest to that of normal whole blood. The constant value $\sqrt{3}C_n = 33.69$ provided the best fit for the first sample and $\sqrt{3}C_n = 33.79$ for the second sample (Fig. 7).

4 Discussion

The empirical value of $\sqrt{3}C_n$ describes 33.69–33.79 greater cell deformation by extensional flow than by shear flow in the range of stress in which the extensional and shear data overlap (about 10–100 Pa). The models of Faghih and Sharp (2019b) for a common energy dissipation rate of 54.4 m^2/s^3 (laminar scalar stress of 12.8 Pa) showed that laminar extensional flow causes 11.9 times greater membrane tension than the RMS value for laminar shear flow. For a common scalar stress of 52 Pa, the same models showed that laminar extensional flow causes 67 times greater membrane tension (Faghih and Sharp 2018a). The relationship between cell deformation and membrane tension can be expected to be nonlinear, as demonstrated by the larger ratio of membrane tension calculated by the models for the higher of the two scalar stresses. For low stress, large changes in aspect ratio occur with small changes in membrane tension, particularly as the biconcave disk shape is stretched to an ellipsoid, but also as the ellipsoid is stretched. For high stress, small changes in aspect ratio produce large changes in membrane tension, particularly as biaxial membrane strain begins. Nonetheless, the similarity of the modeled ratios of membrane tension to the experimental ratio of cell aspect ratios for similar values of fluid stresses provides some qualitative validation.

Only one previous experimental study compared aspect ratio of red cells in extensional flow versus shear flow (Lee et al. 2009). The comparison was made for rabbit blood and for stress levels up to only 3 Pa.[1] For the data of Lee et al.

[1] The stress used here is the axial extensional stress σ_{zz}, whereas Lee et al. (2009) applied the Trouton extensional viscosity (Trouton 1906), which is defined as the ratio of the principal stress difference $\sigma_1 - \sigma_3$ to the extension rate for uniaxial extension, where the subscripts correspond to the principal axes. By continuity for an incompressible fluid, the extension rates along the second and third axes are -1/2 times the extension rate along the first axis. Therefore, for a Newtonian fluid, the Trouton extensional viscosity is 3 times the shear viscosity. For planar extension, such as in the hyperbolic contractions used in this work and that of Lee et al. (2009), there are two extensional viscosities. One, the planar extensional viscosity, is the ratio of $\sigma_1 - \sigma_3$ to the extension rate, which is 4 times the shear viscosity. The second extensional viscosity, or cross-viscosity, is the ratio of $\sigma_2 - \sigma_3$ to the extension rate, where axis 2 is that along which there is zero deformation. The cross-viscosity is 2 times the shear viscosity.

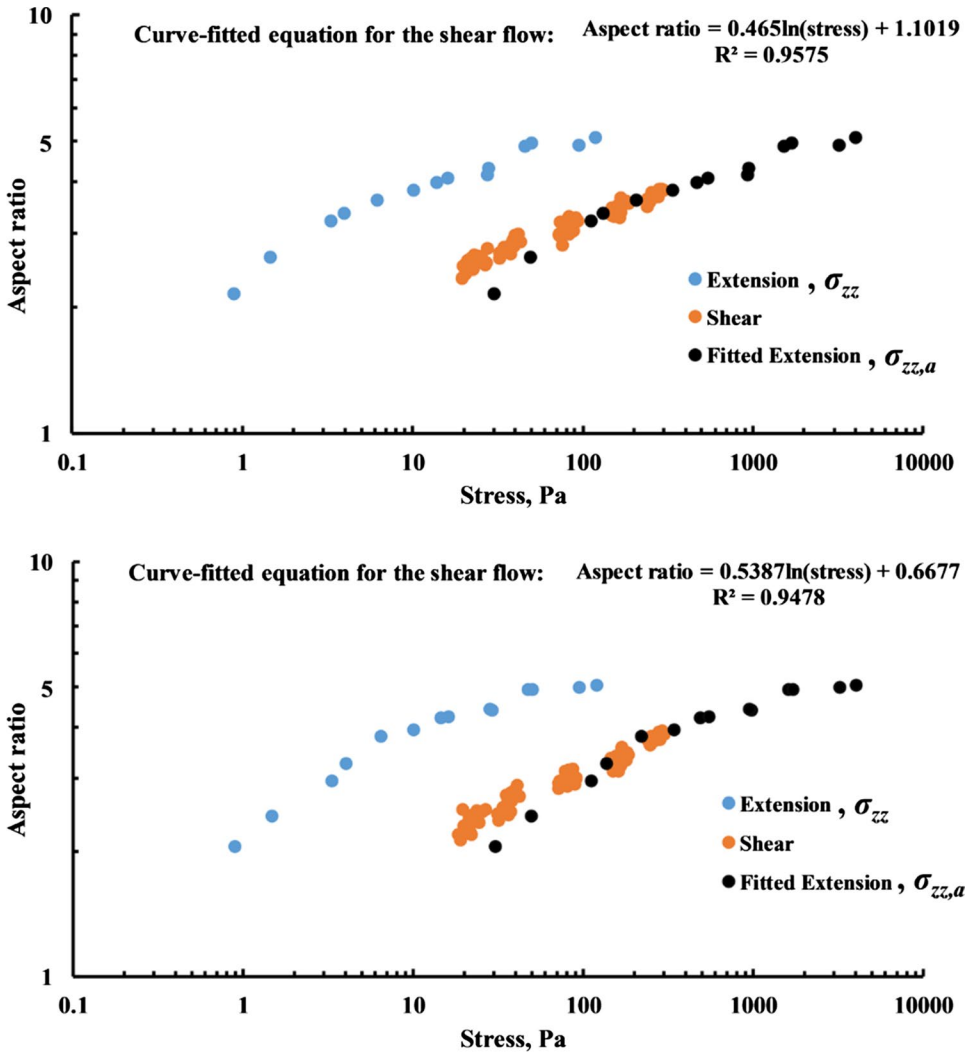

Fig. 7 Rescaling the extensional stress to fit the curve for shear stress, for blood sample 1 (top) and blood sample 2 (bottom). *Note*: Both axes have log scales

(2009), one can calculate the constant $\sqrt{3}C_n$ as 29.1. Thus, these two studies are in substantial agreement that cells are deformed more by extensional stress than by shear stress by approximately an order of magnitude. Results in the present study confirmed this trend for stress levels up to 100 Pa (Fig. 8). Note that the results of the current study shown in Fig. 8 are plotted for the first blood sample, but the second blood sample exhibited the same behavior. This difference in cell deformation might be due to the fact that in extensional flow, the stress acts directly and continuously to pull the cell membrane apart, while in shear flow, the cell membrane rotates around the cytoplasm, thanks to the tank-treading motion, allowing for only a portion of the force to intermittently pull the membrane.

The results of RBC aspect ratio in shear flow (Fig. 6) indicate that higher external viscosity causes larger cell deformation. Pfafferott et al. (1985) also showed that for the same level of shear stress, RBCs are deformed more in a suspending medium of higher viscosity (Fig. 9). Mohandas et al. (1980) found that the relationship between the cell deformation index and shear stress could be normalized by multiplying the shear stress by the square root of viscosity.

Contrary to shear flow, higher external viscosity in extensional flow did not cause a significant increase in cell deformation (Fig. 10). This finding is in general agreement with that of Lee et al. (2009) (also shown in Fig. 10). Nonetheless, there is a mismatch between the two results, in the sense that the curve of the present results is shifted to the right compared to that of Lee et al. (2009). The mismatch could be due to the difference in species, as Lee et al. (2009) used rabbit blood, while human blood was used here. Typical values for diameter and volume for rabbit RBCs are 6.1 μm and 76 μm^3, while they are 7.3 μm and 95 μm^3 for human RBCs (Namdee et al. 2015). Differences in power-law hemolysis coefficients have been confirmed among human, ovine porcine, and bovine cells (Ding et al. 2015). Another possible reason for a mismatch might be that the viscosity of the suspending medium used by Lee et al. (2009) (~31–297 cP) was significantly higher than that used in the current study

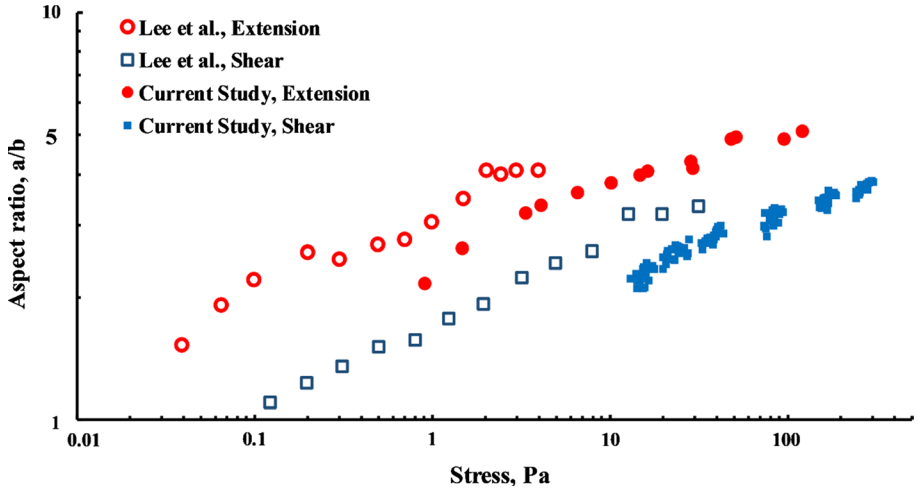

Fig. 8 Results of cell deformation in shear and extensional flows in our study versus Lee et al. (2009). *Note*: Both axes have log scales

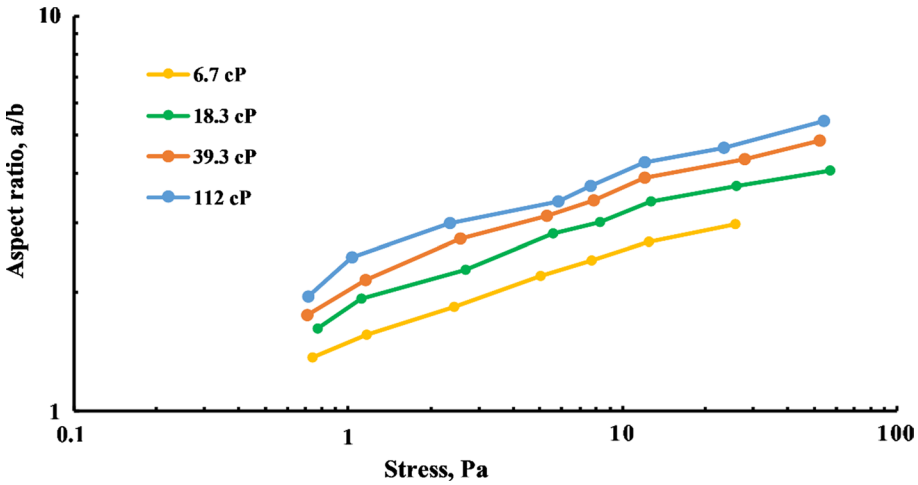

Fig. 9 Aspect ratio of young RBCs versus shear stress for different values of external viscosities, from Pfafferott et al. (1985). *Note*: Both axes have log scales

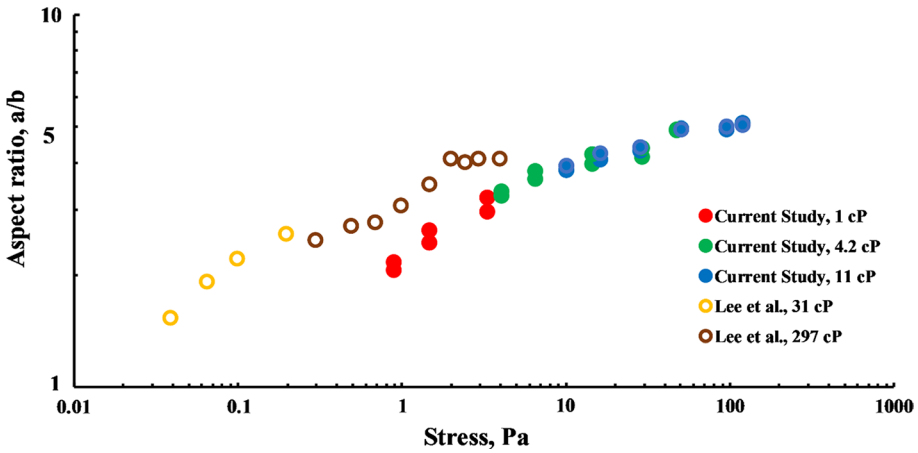

Fig. 10 Aspect ratio of RBCs in planar extensional flow in our study (both samples) and in that of Lee et al. (2009). *Note*: Both axes have log scales

(~ 1–11 cP). While significant differences in deformation by extensional flow were not found in the present study for viscosity in the range 1–11 cP, the effect of much higher viscosity cannot be ruled out.

This difference in behavior of rabbit versus human red cells also suggests that inaccuracies can be expected when results from blood samples other than human are applied for human blood damage prediction. For example, the power-law equation based on data from Heuser and Opitz (1980)

for porcine blood is often used for human blood damage prediction.

4.1 Limitations

There were no limitations associated with leakage of the channel for the purpose of this study. The fabricated channel withstood a pressure of around 350 Pa without any leakage or rupture. However, there were limitations on image quality. Since high pressure was necessary to achieve high flow rates, relatively thick cover plates (0.794 mm) were needed. The thicker cover plates necessitated a longer working distance objective lens, which limited optical performance of the setup and reduced image quality.

No images were obtained of lysed cells for extensional stress up to about 100 Pa. This is consistent with the hemolytic threshold of 3000 Pa proposed by Down et al. (2011) for exposure of microseconds to extensional flow. Greater motor power and/or a more efficient drive mechanism could allow testing at higher flow rates that might produce lysis.

An important conceptual limitation of the model is that cell membrane tension (and by extension, hemolysis) is assumed to scale with global cell deformation, i.e., aspect ratio. While the resulting adjustments to the effective scalar stress can be expected to be a vast improvement over the von Mises-like stress, the correlation has obvious incompleteness when the details of the transfer of fluid stresses to the membrane are considered at the microscale. In particular, the tank-treading cell in shear flow experiences transient stresses that may create short-lived pores that release less hemoglobin than those caused by the continuous tension resulting from extensional stress. At the same aspect ratio, the shape of the cell may also be different depending on the type of stress, which could contribute to a different membrane tension. Further, the circulation of the tank-treading membrane may influence the surrounding fluid motion of shear flow less than that in extensional flow. By adopting a simplified, continuum model, the distribution and time dependence of membrane tension resulting from the full fluid-structure interaction are unresolved. Approaches to incorporate these different responses include multiscale computational solutions and empirical fits of experimental results from hemolytic levels of stress (see Sect. 4.2).

The experiments examined the effects of only two components from the fluid stress tensor [Eq. (6)]. While the proposed representative stress of Eq. (5) includes all components, further experiments are needed to validate the weighting for other stress components and that of combinations of stresses.

Finally, the results were collected and analyzed for only two, aged blood samples. While these two samples produced very similar values for C_n, more data from a larger number of samples would help confirm this result with higher confidence. Results for fresh blood may also yield different values of this weighting factor.

4.2 Future work

Recognizing that deformation (in terms of aspect ratio) may be an imperfect scale for hemolysis, a significant next step would be to conduct experiments to measure hemoglobin release for a wide range of extensional stresses. Such data would validate whether larger cell deformation in extensional flow correlates with greater hemoglobin release.

However, there is a technical challenge in measuring hemoglobin release in extensional flow. In contrast to pure shear, for which devices such as the cone and plate viscometer apply constant shear throughout the device, no device exists that applies constant extensional stress throughout the entire flow domain. An alternative would be to use the aspirator setup of Sallam and Hwang (1984) to sample pathlines with constant extensional stress, for instance, along the centerline of a hyperbolic contraction. Their technique uses an injector placed at an upstream location to release cells in the middle of the channel. Then, an aspirator is used downstream of the contraction to collect the blood samples, for which hemoglobin content can be determined. This technique could also be used to study combinations of extensional and shear stresses by placing and collecting samples on other pathlines not in the center or the contraction.

5 Conclusion

There has been a great deal of literature, both experimental and numerical, on behavior of red cells under pure shear flow (Dupire et al. 2012; Fedosov et al. 2010). However, to develop a universal and accurate hemolysis model, it is equally important to understand the modes of motion and failure of red cell membranes under extensional flow. To the best of the authors' knowledge, this study is the first to compare the deformation of human RBCs in extensional flow to that in shear flow for high stresses within about an order of magnitude of the threshold for membrane failure. Results of the experiments showed that the red cells are deformed significantly more in extensional flow than in shear flow, at the same stress level. Based on these observations, a new representative stress is proposed [Eq. (5)] that adopts scaling matched to the experimental deformation results by weighting extensional stress more than shear stress. This is in contrast to previous scalar stresses [e.g., Eqs. (3) and (4)], which weigh shear stress more than extensional stress.

References

Basu H, Dharmadhikari AK, Dharmadhikari JA, Sharma S, Mathur D (2011) Tank treading of optically trapped red blood cells in shear flow. Biophys J 101:1604–1612. https://doi.org/10.1016/j.bpj.2011.08.043

Blackshear PLJ, Dorman FD, Steinbach JH (1965) Some mechanical effects that influence hemolysis. ASAIO J 11:112–117

Bludszuweit C (1995) Model for a general mechanical blood damage prediction. Artif Organs 19:583–589

Brown CHI, Lemuth RF, Hellums JD, Leverett LB, Alfrey CP (1975) Response of human platelets to shear stress. ASAIO J 21:35–39

Chen Y, Sharp MK (2011) A strain-based flow-induced hemolysis prediction model calibrated by in vitro erythrocyte deformation measurements. Artif Organs 35:145–156. https://doi.org/10.1111/j.1525-1594.2010.01050.x

Ding J, Niu S, Chen Z, Zhang T, Griffith BP, Wu ZJ (2015) Shear-induced hemolysis: species differences. Artif Organs 39:795–802. https://doi.org/10.1111/aor.12459

Down LA, Papavassiliou DV, O'Rear EA (2011) Significance of extensional stresses to red blood cell lysis in a shearing flow. Ann Biomed Eng 39:1632–1642. https://doi.org/10.1007/s10439-011-0262-0

Dupire J, Socol M, Viallat A (2012) Full dynamics of a red blood cell in shear flow. Proc Natl Acad Sci USA 109:20808–20813. https://doi.org/10.1073/pnas.1210236109

Faghih MM, Sharp MK (2016) Extending the power-law hemolysis model to complex flows. J Biomech Eng 138:12. https://doi.org/10.1115/1.4034786

Faghih MM, Sharp MK (2018a) Characterization of erythrocyte membrane tension for hemolysis prediction in complex flows. Biomech Model Mechanobiol 17:827–842. https://doi.org/10.1007/s10237-017-0995-2

Faghih MM, Sharp MK (2018b) Solvent-based bonding of PMMA-PMMA for microfluidic applications. Microsyst Technol. https://doi.org/10.1007/s00542-018-4266-7

Faghih MM, Sharp MK (2019a) Modeling and prediction of flow-induced hemolysis: a review. Biomech Model Mechanobiol. https://doi.org/10.1007/s10237-019-01137-1

Faghih MM, Sharp MK (2019b) Evaluation of energy dissipation rate as a predictor of mechanical blood damage. Artif Organs 43:666–676. https://doi.org/10.1111/aor.13418

Fedosov DA, Caswell B, Karniadakis GE (2010) A multiscale red blood cell model with accurate mechanics, rheology, and dynamics. Biophys J 98:2215–2225. https://doi.org/10.1016/j.bpj.2010.02.002

Fischer TM (2007) Tank-tread frequency of the red cell membrane: dependence on the viscosity of the suspending medium. Biophys J 93:2553–2561. https://doi.org/10.1529/biophysj.107.104505

Fischer TM, Stohr-Lissen M, Schmid-Schonbein H (1978) The red cell as a fluid droplet: tank tread-like motion of the human erythrocyte membrane in shear flow. Science 202:894–896

Giersiepen M, Krause U, Knott E, Reul H, Rau G (1989) Velocity and shear stress distribution downstream of mechanical heart valves in pulsatile flow. Int J Artif Organs 12:261–269

Heuser G, Opitz R (1980) A Couette viscometer for short time shearing of blood. Biorheology 17:17–24

Keshaviah PR (1976) Hemolysis in the accelerated flow region of an abrupt contraction. PhD thesis, University of Minnesota

Khoo DPY, Cookson AN, Gill HS, Fraser KH (2018) Normal fluid stresses are prevalent in rotary ventricular assist devices: a computational fluid dynamics analysis. Intl J Artif Organs 41(11):738–751

Laugel JF, Beissinger RL (1983) Low stress shear-induced hemolysis in capillary flow. Trans Am Soc Artif Intern Organs 29:158–162

Lee SS, Yim Y, Ahn KH, Lee SJ (2009) Extensional flow-based assessment of red blood cell deformability using hyperbolic converging microchannel. Biomed Microdevices 11:1021–1027. https://doi.org/10.1007/s10544-009-9319-3

Leverett LB, Hellums JD, Alfrey CP, Lynch EC (1972) Red blood cell damage by shear stress. Biophys J 12:257–273

Mohandas N, Clark MR, Jacobs MS, Shohet SB (1980) Analysis of factors regulating erythrocyte deformability. J Clin Invest 66:563–573

Namdee K, Carrasco-Teja M, Fish MB, Charoenphol P, Eniola-Adefeso O (2015) Effect of variation in hemorheology between human and animal blood on the binding efficacy of vascular-targeted carriers. Sci Rep 5:11631. https://doi.org/10.1038/srep11631

Nevaril CG, Lynch EC, Alfrey CP Jr, Hellums JD (1968) Erythrocyte damage and destruction induced by shearing stress. J Lab Clin Med 71:784–790

Ober TJ, Haward SJ, Pipe CJ, Soulages J, McKinley GH (2013) Microfluidic extensional rheometry using a hyperbolic contraction geometry. Rheol Acta 52:529–546

Oliveira M, Alves MA, Pinho FT, McKinley GH (2007) Viscous fluid flow through microfabricated hperbolic contractions. Exp Fluids 43:437–451. https://doi.org/10.1007/s00348-007-0306-2

Pfafferott C, Nash GB, Meiselman HJ (1985) Red blood cell deformation in shear flow. Effects of internal and external phase viscosity and of in vivo aging. Biophys J 47:695–704. https://doi.org/10.1016/S0006-3495(85)83966-7

Richardson E (1974) Deformation and haemolysis of red cells in shear flow. Proc R Soc Lond A Math Phys Eng Sci 338:129–153. https://doi.org/10.1098/rspa.1974.0078

Sallam AM, Hwang NH (1984) Human red blood cell hemolysis in a turbulent shear flow: contribution of Reynolds shear stresses. Biorheology 21:783–797

Sousa PC, Pinho FT, Oliveira MS, Alves MA (2011a) Extensional flow of blood analog solutions in microfluidic devices. Biomicrofluidics 5:14108. https://doi.org/10.1063/1.3567888

Sousa PC, Pinho IS, Pinho FT, Oliveira MSN, Alves MA (2011b) Flow of a blood analogue solution through microfabricated hyperbolic contractions. In: Tavares SJMR, Jorge NRM (eds) Computational vision and medical image processing: recent trends. Springer, Dordrecht, pp 265–279. https://doi.org/10.1007/978-94-007-0011-6_15

Tran-Son-Tay R, Sutera SP, Zahalak GI, Rao PR (1987) Membrane stress and internal pressure in a red blood cell freely suspended in a shear flow. Biophys J 51:915–924. https://doi.org/10.1016/s0006-3495(87)83419-7

White FM (1991) Viscous fluid flow. McGraw-Hill, New York

Yen J-H, Chen S-F, Chern M-K, Lu P-C (2015) The effects of extensional stress on red blood cell hemolysis. Biomed Eng Appl Basis Commun 27:1550042. https://doi.org/10.4015/S1016237215500428

Zhang T, Taskin ME, Fang H-B, Pampori A, Jarvik R, Griffith BP, Wu ZJ (2011) Study of flow-induced hemolysis using novel Couette-type blood-shearing devices. Artif Organs 35:1180–1186. https://doi.org/10.1111/j.1525-1594.2011.01243.x